Expanded View Figures

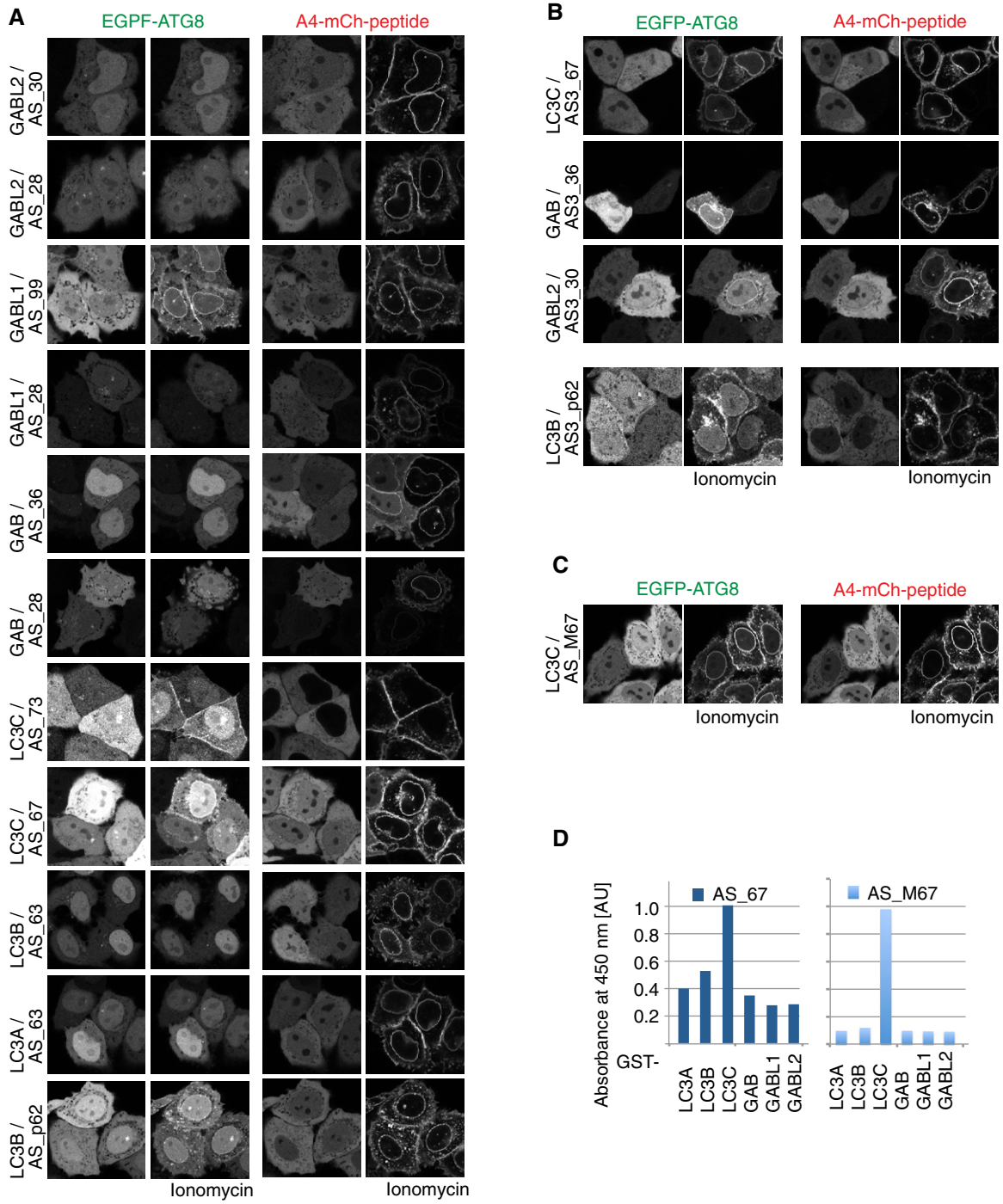

Figure EV1. Cellular validation of ATG8 sensors.

A–C Annexin A4-based co-translocation assays of peptide binders and EGFP-mATG8. Triplication of peptides (B) or introduction of negative charges in close proximity to the binding motif (C) increases the potential of peptide binders to co-translocate their target mATG8.

D Biotinylated octameric peptides representing a single amino acid walk-through along the complete 16-mer peptide AS_67 and AS_M67 are immobilized on streptavidin. Binding of GST-ATG8 fusion protein to the immobilized peptides is detected by a GST-specific antibody (HRP-conjugated) and shown as absorbance at 450 nm. AU = arbitrary unit.

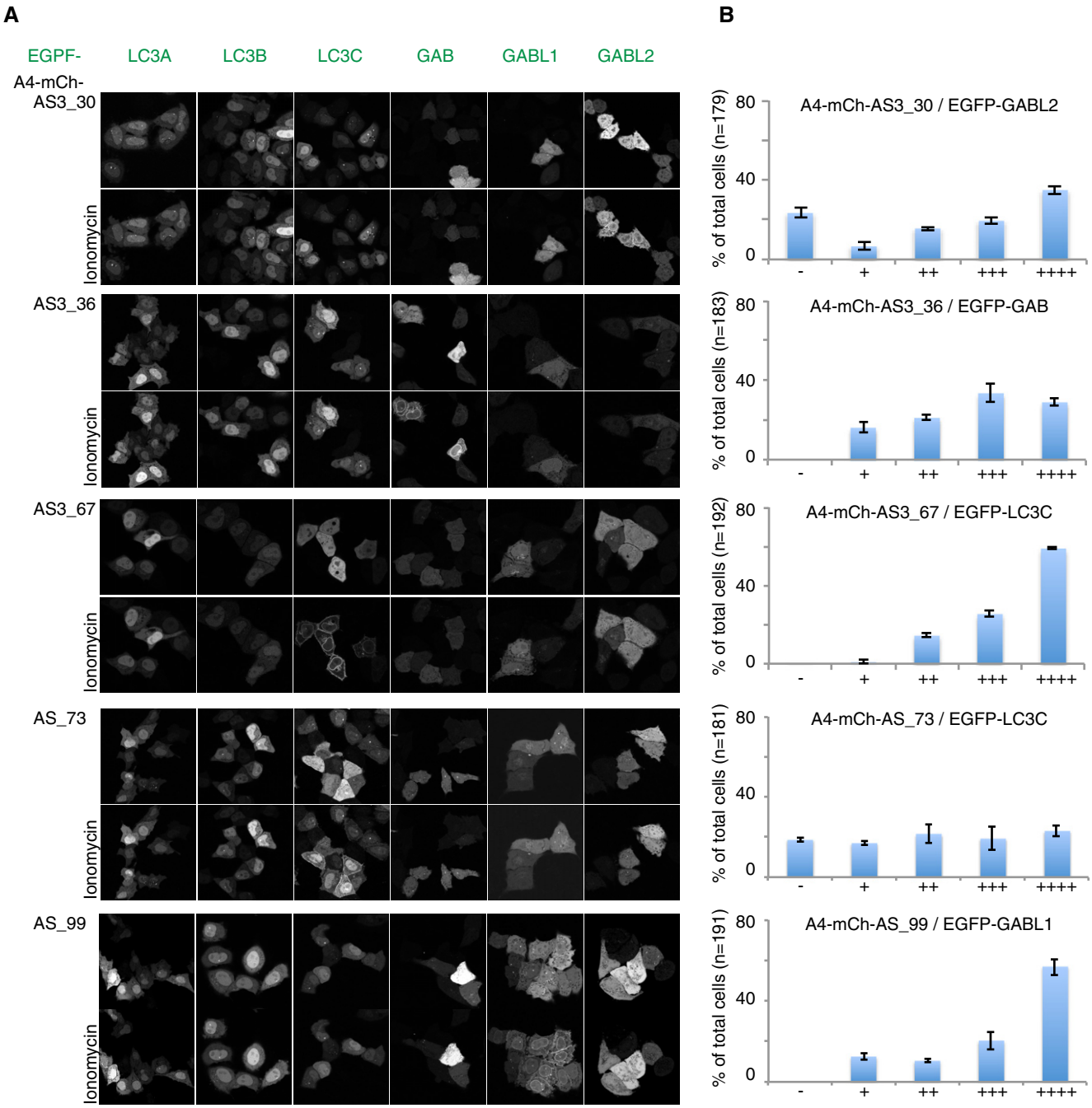

Figure EV2. Cellular validation of ATG8 sensors.

A Annexin A4-based co-translocation assays of peptide binders and EGFP-mATG8. mATG8 peptide binders specifically co-translocate their target-mATG8, while non-cognate mATG8s remain cytosolic upon ionomycin treatment.

B Quantification of the translocation potential of peptide binders for their target mATG8. Combined data from three biological replicates are presented. Number of counted cells per experiment > 50. Classification ranges from "–" (no translocation) to "++++" (very good); *n* = total number of counted cells. Error bars represent ± SD.

Figure EV3. ATG8 sensors are specific for autophagosomes decorated with cognate mATG8.

A mCh-AS3_p62, mCh-AS3_67, and mCh-AS2_10M30 are assayed for specificity toward all six mATG8s. Experiments were performed in HeLa cells stably expressing indicated sensor after doxycycline induction. Scale bar: 10 μm.

B Quantification of experiments presented in (B) and Fig 3D. Number of counted cells/autophagosomes is provided for each experiment.

C Sensor mCh-AS3_30 is instable. Stable inducible HeLa cell lines expressing indicated sensor were treated with indicated compounds and analyzed by immunoblot with antibodies against mCherry. MG132 treatment stabilizes the sensor, as it is apparent in the overexposed blot (red arrow).

D ITC experiments showed significant preference of the Ub19-AS_30 fusion construct to GABARAPL2 (K_D 0.8 μM, ΔH −15.0 kcal/mol, and ΔS −22.3 cal/mol/K) over LC3A (K_D ~10 μM, ΔH −3.4 kcal/mol, and ΔS +12.4 cal/mol/K). Top panels display the raw heat per injection, and the lower panels display the integrated heat per titration over molar ratio (protein: Ub19-AS_30) with correction to heat of dilution. K_D values determined in assumption of "one site interaction" are given for each experiment. These parameters were mirrored in NMR experiments presented in (E).

E Titration of Ub19-AS_30 fusion construct to ^{15}N-labeled LC3B (upper plot) indicates weak interaction with intermediate exchange mode, while that for GABARAPL2 (lower plot) shows strong interaction in slow exchange mode. Representative sections of ^{1}H-^{15}N HSQC spectra for ^{15}N-labeled proteins (LC3B and GABARAPL2) upon titration with Ub19-AS_30 fusion construct are shown in overlay. Both plots show "fingerprint regions" of the proteins spectra (around HN resonance of K51 in LC3A and LC3B, which is K57 in LC3C and K48 in all GABARAP proteins). Resonances of LC3B and GABARAPL2 proteins in their free states and in the presence of 0.25 and 2.0 molar ratios of Ub19-AS_30 fusion construct are red and yellow and blue, respectively. Resonance assignments are given where necessary in red for free state and blue for Ub19-AS_30-saturated state. Changes in positions of resonances due to interaction with AS_30 are highlighted with dashed arrows.

F Peptide array analysis of single amino acid walk-through with octameric peptides along the complete 16-mer of peptide binder AS_30 against GST-GABL2. AU = arbitrary unit.

G Immunofluorescence of EGFP-AS3_73 expressed in HeLa cells revealed recruitment of the sensor to subcellular structures under basal conditions.

Source data are available online for this figure.

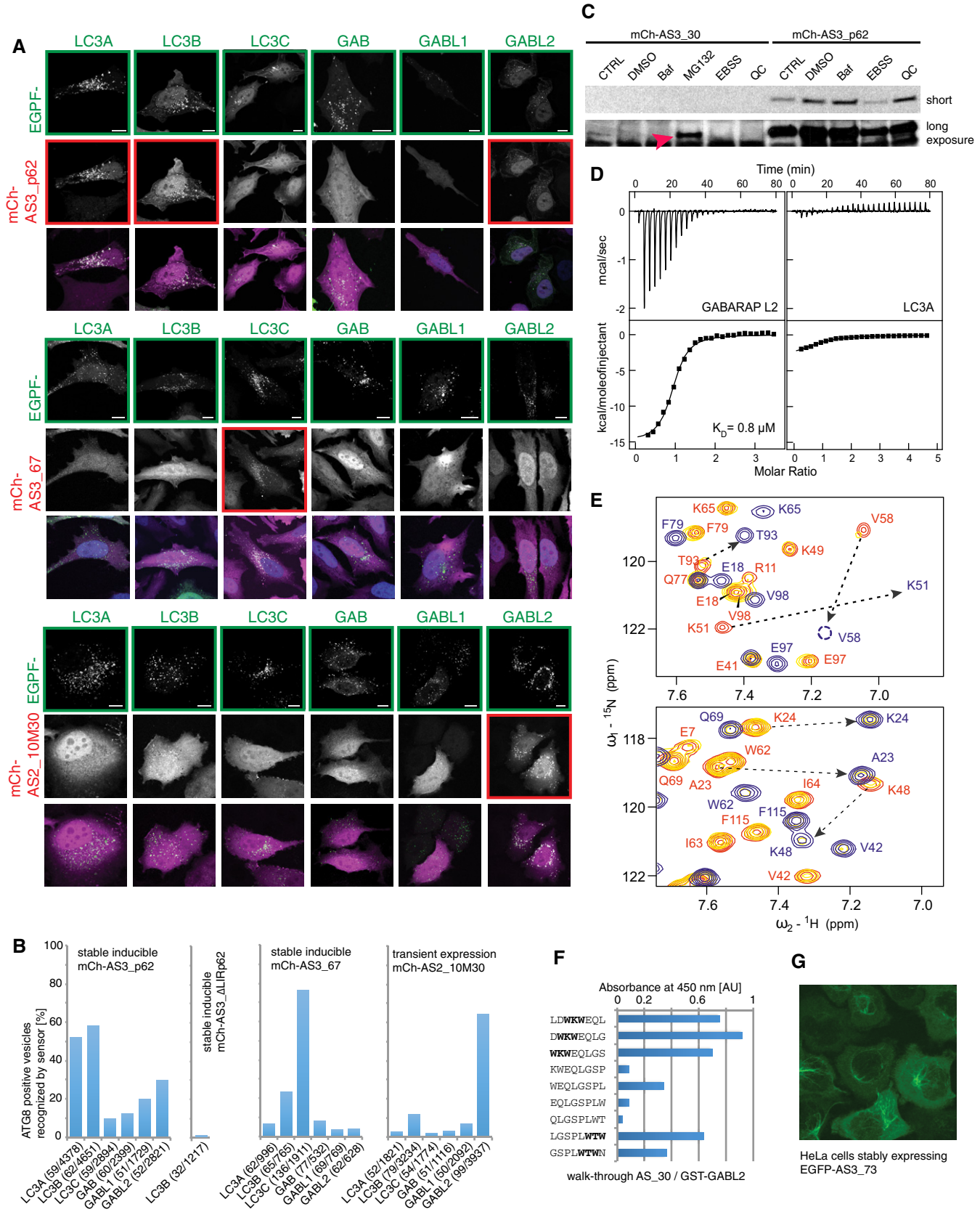

Figure EV3.

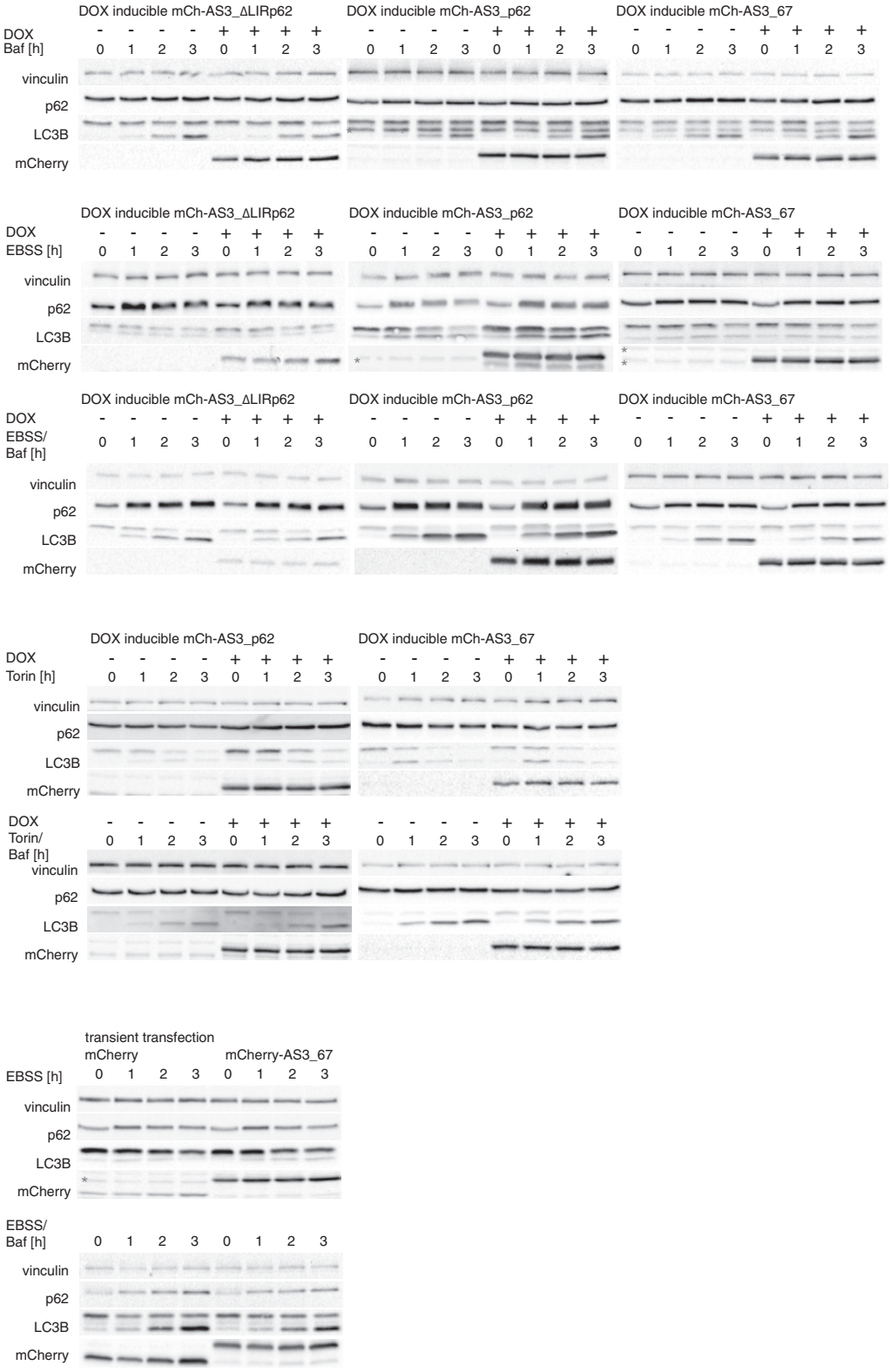

Figure EV4. Autophagy flux in the absence and presence of ATG8 sensors.
Analysis of autophagy flux in stable inducible HeLa cells expressing mCherry fusions of indicated ATG8 sensor upon doxycycline (DOX) induction or in HEK293T cells expressing indicated ATG8 sensor upon transient transfection. Representative images for quantifications of Fig EV5 are shown. Asterisk indicates unspecific binding of the antibody.

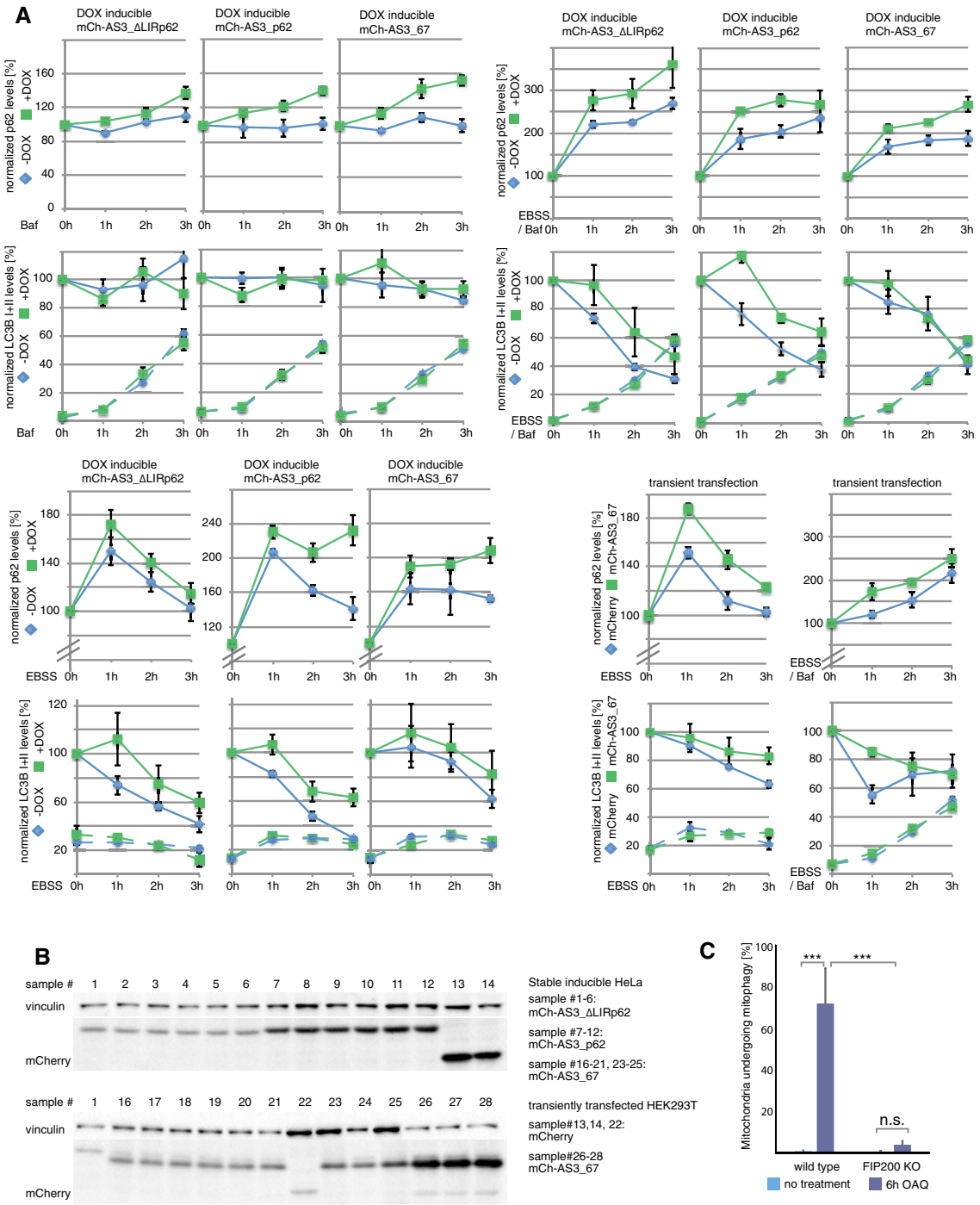

Figure EV5. Quantification of autophagy flux in the absence and presence of ATG8 sensors.

A Quantification of autophagy flux data shown in Fig EV4. Normalized levels of LC3B I and II are represented by continuous and dashed lines, respectively. Data present the mean of three independent experiments ± SEM.

B Comparison of the expression levels of sensors. 3 h samples of experiments presented in Fig EV4 were loaded and detected with anti-tRFP antibody. Numbers above gel lanes assign individual samples to cells expressing indicated constructs.

C FACS-based mitophagy flux analysis performed in wild-type and FIP200 KO cells stably expressing HA-Parkin and mt-mKeima. Cells were treated with OAQ (oligomycin, antimycin, Q-VD) for the indicated times and analyzed by FACS for lysosomal-positive mt-mKeima (561 nm). The average of three independent experiments is presented. Error bars indicate standard deviation. Significance calculation: one-way ANOVA. n.s. = not significant. *** indicates *P*-value of 0.0001.

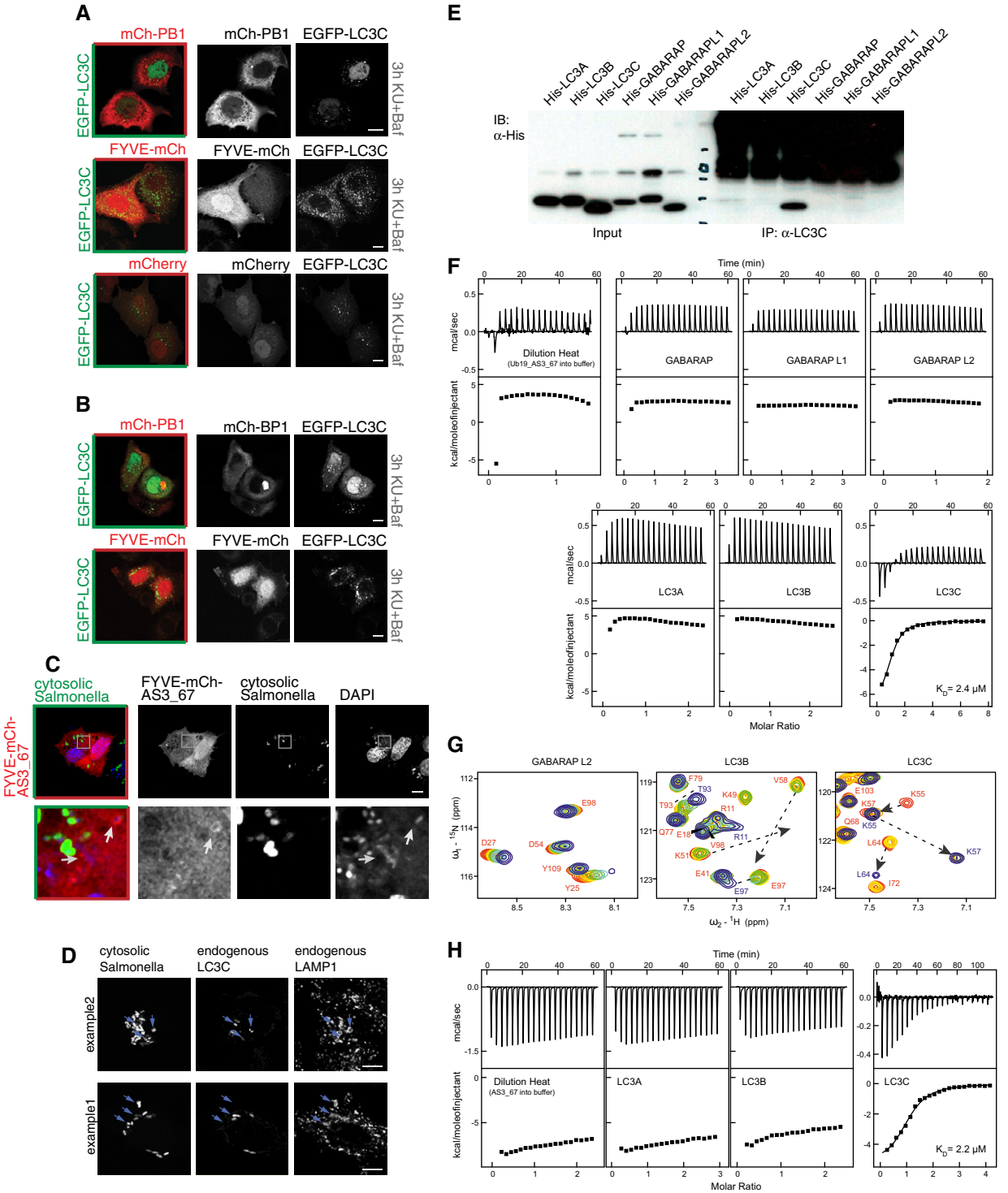
A
mCh-PB1
mCh-PB1
EGFP-LC3C
EGFP-LC3C
3h KU+Baf
FYVE-mCh
FYVE-mCh
EGFP-LC3C
mCherry
mCherry
EGFP-LC3C
B
mCh-PB1
mCh-BP1
EGFP-LC3C
FYVE-mCh
FYVE-mCh
EGFP-LC3C
C
cytosolic Salmonella
FYVE-mCh-AS3_67
cytosolic Salmonella
DAPI
FYVE-mCh-AS3_67
D
cytosolic Salmonella
endogenous LC3C
endogenous LAMP1
example2
example1
E
His-LC3A
His-LC3B
His-LC3C
His-GABARAP
His-GABARAPL1
His-GABARAPL2
IB: α-His
Input
IP: α-LC3C
F
Time (min)
mcal/sec
kcal/moleofinjectant
Dilution Heat
(Ub19_AS3_67 into buffer)
GABARAP
GABARAP L1
GABARAP L2
LC3A
LC3B
LC3C
K_D = 2.4 μM
Molar Ratio
G
GABARAP L2
LC3B
LC3C
ω1 - 15N (ppm)
ω2 - 1H (ppm)
H
Time (min)
mcal/sec
kcal/moleofinjectant
Dilution Heat
(AS3_67 into buffer)
LC3A
LC3B
LC3C
K_D = 2.2 μM
Molar Ratio

Figure EV6.

Figure EV6. Specificity of ATG8 sensors.

A, B Control experiments for data presented in Figs 5 and 6. mCherry, as well as the fusion proteins mCherry-PB1 and FYVE-mCherry, does not localize to autophagosomes positive for overexpressed EGFP-LC3C. Scale bar: 10 μm.

C High-performance sensor FYVE-mCh-AS3_67 was transiently expressed in *Salmonella*-infected HeLa cells to monitor xenophagy events. Even though the sensor was recruited to cytosolic *Salmonella* to certain extent, its performance fell short of sensor mCh-PB1-AS3_67. Scale bar: 10 μm.

D A subpopulation of cytosolic *Salmonella* is coated with endogenous LC3C and engulfed by lysosomes in HeLa cells (marker: endogenous LAMP1). Arrows indicate examples of *Salmonella* located within lysosomes. Scale bar: 10 μm.

E LC3C-specific antibody (Stadel *et al*, 2015) was incubated with purified, recombinant HIS6 fusion proteins of mATG8s and subsequently subjected to immunoprecipitation (IP) experiments with protein A–Sepharose. The specificity of the antibody for LC3C was confirmed. Unspecific signal in the high molecular weight area of the IP samples is caused by the LC3C antibody.

F ITC experiments showed significant preference of Ub19-AS_67 fusion construct to LC3C. Titrations of all other human ATG8 proteins with Ub19-AS_67 fusion construct revealed weak interactions and do not differ significantly from Ub19-AS_67 dilution heat. In contrast, titration of LC3C with Ub19-AS_67 fusion construct shows a relatively strong interaction (K_D 2.4 μM, ΔH −7.2 kcal/mol, and ΔS +1.4 cal/mol/K) comparable to that for p62 and NBR1 LIR interactions to LC3B (Rozenknop *et al*, 2011). Top panels display the raw heat per injection, and the lower panels display the integrated heat per titration over molar ratio (protein: Ub19-AS_67).

G NMR titration of Ub19-AS_67 fusion construct to ^{15}N-labeled GABARAPL2, LC3B, and LC3C proteins shows its specificity for LC3C. NMR titration of Ub19-AS_67 fusion construct to ^{15}N-labeled GABARAPL2 (left plot) and LC3B (middle plot) indicates weak interactions with an intermediate exchange mode, while that for LC3C shows a stronger interaction in slow exchange mode. Representative sections of ^{1}H-^{15}N HSQC spectra for ^{15}N-labeled proteins upon titration with Ub19-AS_67 fusion construct are shown in overlay. All plots show "fingerprint regions" of the proteins spectra (around HN resonance of K51 in LC3B, K48 in GABARAPL2, and K57 in LC3C). Molar ratios of protein: Ub19-AS_67 are rainbow-color-coded (1:0, 1:0.25, 1:0.5, 1:1, 1:2; red to blue) for each titration step. Changes in positions of resonances due to interaction with AS_67 are highlighted with dashed arrows.

H ITC experiments showed significant preference of AS_67 peptide to LC3C. Similar to Ub19-AS_67 fusion construct, de-tagged AS_67 peptide did not show significant interaction with LC3A and LC3B proteins. Corresponding titration profiles are very similar to dilution heat of the peptides. In contrast, AS_67 peptide interacts with LC3C protein, and ITC analysis results are similar to Ub19-AS_67 parameters of interaction (K_D 2.2 μM, ΔH −5.4 kcal/mol, and ΔS +7.8 cal/mol/K). Top panels display the raw heat per injection, and the lower panels display the integrated heat per titration over molar ratio (protein: AS_67).